

Structure Functions for Light Nuclei

S. A. Kulagin^{1,*} and R. Petti^{2,†}

¹*Institute for Nuclear Research of the Russian Academy of Sciences, 117312 Moscow, Russia*

²*Department of Physics and Astronomy,
University of South Carolina, Columbia SC 29208, USA*

Abstract

We discuss the nuclear EMC effect with particular emphasis on recent data for light nuclei including ${}^2\text{H}$, ${}^3\text{He}$, ${}^4\text{He}$, ${}^9\text{Be}$, ${}^{12}\text{C}$ and ${}^{14}\text{N}$. In order to verify the consistency of available data, we calculate the χ^2 deviation between different data sets. We find a good agreement between the results from the NMC, SLAC E139, and HERMES experiments. However, our analysis indicates an overall normalization offset of about 2% in the data from the recent JLab E03-103 experiment with respect to previous data for nuclei heavier than ${}^3\text{He}$. We also discuss the extraction of the neutron/proton structure function ratio F_2^n/F_2^p from the nuclear ratios ${}^3\text{He}/{}^2\text{H}$ and ${}^2\text{H}/{}^1\text{H}$. Our analysis shows that the E03-103 data on ${}^3\text{He}/{}^2\text{H}$ require a renormalization of about 3% in order to be consistent with the F_2^n/F_2^p ratio obtained from the NMC experiment. After such a renormalization, the ${}^3\text{He}$ data from the E03-103 data and HERMES experiments are in a good agreement. Finally, we present a detailed comparison between data and model calculations, which include a description of the nuclear binding, Fermi motion and off-shell corrections to the structure functions of bound proton and neutron, as well as the nuclear pion and shadowing corrections. Overall, a good agreement with the available data for all nuclei is obtained.

arXiv:1004.3062v2 [hep-ph] 24 Dec 2010

* kulagin@ms2.inr.ac.ru

† Roberto.Petti@cern.ch

I. INTRODUCTION

The nuclear EMC effect in the deep-inelastic scattering (DIS) has been discussed since early 1980s starting from the observation of a dramatic change in the structure function of a heavy nucleus relative to that of the deuteron [1]. The nuclear effects in DIS were experimentally measured in the form of the ratio $\mathcal{R}(A/B) = F_2^A/F_2^B$ of the structure functions (or the cross sections) of two nuclei (usually a complex nucleus to deuterium) in the experiments at CERN [2–6], SLAC [7], DESY [8], FNAL [9]. The data were taken for different nuclear targets and at different regions of the Bjorken x and the invariant momentum transfer squared Q^2 and significant nuclear effects were observed (for a review see [10, 11]). Recently, the E03-103 experiment at Jlab published a high-statistics measurements of the EMC effect for ${}^3\text{He}$, ${}^4\text{He}$, ${}^9\text{Be}$, and ${}^{12}\text{C}$, nuclei emphasizing the region of large x [12]. In this article we discuss the statistical consistency of data sets from different experiments collected with the same nuclear targets in the region $0.1 < x < 0.7$, focusing on the kinematical region and the targets used in the E03-103 experiment. We also study the sensitivity of the data on the EMC effect in ${}^3\text{He}$ to the modeling of the ratio F_2^n/F_2^p .

A quantitative understanding the nuclear effects in DIS is important for a number of reasons. A proper interpretation of experimental data can provide valuable insights into the origin of nuclear force and helps us to understand how the properties of hadrons modify in a nuclear medium. It should be also noted that the nuclear data often serve as the source of information on hadrons otherwise not directly accessible. A typical example is the extraction of the neutron structure function which is usually obtained from deuterium and proton data and requires a detailed knowledge of nuclear effects [13]. Other examples include the using of charged-lepton and neutrino nuclear data in global QCD fits aiming to better determine the proton and neutron parton distribution functions and the higher twist terms [14–16]. Understanding the nuclear effects is particularly relevant for precision measurements in neutrino physics, where heavy nuclear targets are used in order to collect a significant number of interactions.

A quantitative model for nuclear structure functions was recently developed in Refs.[17, 18]. This approach accounts for a number of nuclear effects including nuclear Fermi motion and binding (FMB), nuclear pion excess, shadowing, and off-shell correction to bound nucleon structure functions. The detailed analysis of data published before 1996 on the ratios $\mathcal{R}(A/B)$ for a wide region of nuclear targets shows a good performance of the model which was able to describe the observed x , Q^2 , and A dependencies [17]. In the present article we compare the predictions of our model with the recent data from HERMES [8] and E03-103 [12] experiments and discuss the role of different nuclear corrections in light nuclei.

The article is organized as follows. In Sec.II we outline the model used in our studies. In Sec.III we discuss the data from different experiments and also confront the results of our calculation with data. In Sec.IV we summarize the results.

II. THEORETICAL MODEL

We recall that while DIS is characterized by a large invariant momentum transfer $Q \gg M$, where M is the nucleon mass, the characteristic longitudinal distance in the target rest frame $L \sim 2q_0/Q^2 = (Mx)^{-1}$ is not small in hadronic scale (see, *e.g.*, Ref.[19]). In nuclei, the comparison between L and an average distance between bound nucleons r_{NN} gives the characteristic regions of the Bjorken variable x , which are governed by different nuclear

effects. As $r_{NN} \sim 1 \div 2$ fm, at large values of x we have $L \ll r_{NN}$ and nuclear DIS can be approximated by the incoherent scattering off the bound protons and neutrons (impulse approximation, or IA). In this region the major nuclear corrections are due to nuclear binding and nucleon momentum distribution (Fermi motion). At small values of x the longitudinal distance L becomes large and the IA is difficult to justify. In this region the corrections due to scattering off nuclear pions (meson exchange currents), as well as the nuclear (anti-)shadowing effect due to coherent multiple interactions of hadronic component of virtual intermediate boson with bound nucleons, become important. Summarizing, for the nuclear structure function we have different contributions (to be specific we discuss F_2 , for more detail see Ref.[17]):

$$F_2^A = F_2^{(IA)} + \delta_\pi F_2^A + \delta_{\text{coh}} F_2^A, \quad (1)$$

where the first term in the right-hand side stands for the impulse approximation, and $\delta_\pi F_2$ and $\delta_{\text{coh}} F_2$ are the corrections due to scattering off the nuclear pion (meson) field and the coherent interaction of the intermediate virtual boson with the nuclear target, respectively.

The IA term dominates at large x . This term can be written as a sum of the proton ($\tau = p$) and the neutron ($\tau = n$) contributions [17]:

$$\gamma^2 F_2^A(x, Q^2) = \sum_{\tau=p,n} \int [dp] \mathcal{P}^\tau(\varepsilon, \mathbf{p}) \left(1 + \frac{\gamma p_z}{M}\right) \left(\gamma'^2 + \frac{6x'^2 \mathbf{p}_\perp^2}{Q^2}\right) F_2^\tau(x', Q^2, p^2), \quad (2)$$

where the integration is taken over the four-momentum of the bound nucleon $p = (M + \varepsilon, \mathbf{p})$ and $[dp] = d\varepsilon d^3\mathbf{p}/(2\pi)^4$. In the integrand, $\mathcal{P}^{p(n)}(\varepsilon, \mathbf{p})$ is the proton (neutron) nuclear spectral function, which describes the energy and momentum distribution of bound nucleons, $F_2^{p(n)}$ is the structure function of bound proton (neutron), which depends on the Bjorken variable $x' = Q^2/(2pq)$ the momentum transfer square Q^2 and also on the nucleon invariant mass squared $p^2 = (M + \varepsilon)^2 - \mathbf{p}^2$. In Eq.(2) we use the coordinate system in which the momentum transfer \mathbf{q} is antiparallel to the z axis, \mathbf{p}_\perp is the transverse component of the nucleon momentum, and $\gamma^2 = 1 + 4x^2 M^2/Q^2$ and $\gamma'^2 = 1 + 4x'^2 p^2/Q^2$.

Nuclei typically have different proton and neutron numbers. For this reason the nuclear structure functions generally have both the isoscalar and the isovector contributions. In order to separate the isoscalar and isovector contributions in Eq.(2), we introduce the isoscalar $\mathcal{P}^{p+n} = \mathcal{P}^p + \mathcal{P}^n$ and the isovector $\mathcal{P}^{p-n} = \mathcal{P}^p - \mathcal{P}^n$ spectral functions. The spectral function \mathcal{P}^{p+n} is normalized to the total nucleon number $A = Z + N$ with Z and N being the proton and neutron number, respectively, and \mathcal{P}^{p-n} is normalized to $Z - N$. We separate the normalizations from the spectral functions and write

$$\mathcal{P}^{p+n} = A\mathcal{P}_0, \quad (3a)$$

$$\mathcal{P}^{p-n} = (Z - N)\mathcal{P}_1, \quad (3b)$$

where the reduced spectral functions \mathcal{P}_0 and \mathcal{P}_1 are both normalized to unity. Using Eq.(3) we explicitly write the nuclear structure function in Eq.(2) in terms of the isoscalar and the isovector contributions

$$F_2^A/A = \langle F_2^N \rangle_0 + \frac{\beta}{2} \langle F_2^{p-n} \rangle_1, \quad (4)$$

where $F_2^N = \frac{1}{2}(F_2^p + F_2^n)$ is the structure function of the isoscalar nucleon and $F_2^{p-n} = F_2^p - F_2^n$ and the parameter $\beta = (Z - N)/A$ describes the fractional difference of protons and neutrons in a nucleus. The quantities $\langle F \rangle_0$ and $\langle F \rangle_1$ are the contracted notations of the integration

in Eq.(2) taken with the reduced spectral functions \mathcal{P}_0 and \mathcal{P}_1 , respectively. The model of \mathcal{P}_0 and \mathcal{P}_1 , which is used in this article for nuclei with $A \geq 4$, is discussed in Sec.II A. We also note that for ${}^3\text{He}$ we apply Eq.(2) with the proton and neutron spectral functions taken from microscopic calculations of Refs.[21, 23].

It should be noted that the experimental data on the nuclear EMC effect have been often presented for the isoscalar part of the nuclear structure functions in order to facilitate comparison between different nuclei. In order to separate the isoscalar part from nuclear data, a common practice is to multiply the data by a factor

$$C_{is} = \frac{AF_2^N}{ZF_2^p + NF_2^n} = \left(1 - \beta \frac{F_2^{p-n}}{F_2^{p+n}}\right)^{-1} \quad (5)$$

that accounts for the proton-neutron difference in a nuclear target. Indeed, neglecting nuclear effects we have from Eq.(4) $C_{is}F_2^A = AF_2^N$. It must be emphasized, however, that this method is only an approximate way to isolate the isoscalar contribution to the structure functions, as a correct procedure should involve the details of the proton and neutron distributions in nuclei. Also, it is important to realize that the data are biased by this procedure as the factor C_{is} depends on the neutron structure function through the ratio F_2^n/F_2^p and different experiments employ different models of this ratio. For this reason the comparison between theoretical calculations and data is not clear-cut for nonisoscalar nuclei. Apparently, a consistent comparison between data and calculations for nonisoscalar nuclei should involve unbiased data. However, in practice it is not always possible to remove the isoscalar correction from data of specific experiments.

A. Nuclear Spectral Function

The nuclear spectral function \mathcal{P} describes the energy and momentum distributions of bound nucleons and can be written as

$$\mathcal{P}(\varepsilon, \mathbf{p}) = 2\pi \langle A | a^\dagger(\mathbf{p}) \delta(E_A - H - \varepsilon) a(\mathbf{p}) | A \rangle, \quad (6)$$

where $a^\dagger(\mathbf{p})$ and $a(\mathbf{p})$ are creation and annihilation operators of the nucleon with momentum \mathbf{p} , E_A is the energy of the nuclear state $|A\rangle$, and H is the Hamiltonian of the system. Note that we discuss unpolarized scattering and in Eq.(6) we implicitly assume the sum over nucleon polarizations. For simplicity, we also suppress explicit notations for the nucleon isospin state (proton or neutron) of \mathcal{P} and the operators a^\dagger and a .

Note also that Eq.(6) is written in the target rest frame and defines the nuclear spectral function as a function of nucleon energy $\varepsilon = p_0 - M$ and momentum \mathbf{p} . However, in the literature the spectral function is usually considered as a function of the nucleon separation energy E . The spectral function in this case is denoted by $P(E, \mathbf{p})$. The relation between $\mathcal{P}(\varepsilon, \mathbf{p})$ and $P(E, \mathbf{p})$ is driven by a relation between ε and E , which differ by the kinetic energy of a recoil nuclear system of $A-1$ nucleons, $\varepsilon = -E - \mathbf{p}^2/2M_{A-1}$ (for more details see Ref.[20]).

A common way to calculate the spectral function is to insert a full set of the intermediate states in Eq.(6) and evaluate the sum of the corresponding nuclear matrix elements. In the case of the deuteron, the intermediate states reduce to a free proton or neutron, and the spectral function is given entirely in terms of the deuteron wave function square and

$\varepsilon = E_D - \mathbf{p}^2/2M$, where $E_D \approx -2.22$ MeV the deuteron binding energy (the explicit form of Eq.(2) in this case is given in Ref.[17]).

For a ${}^3\text{He}$ nucleus, the proton spectral function receives two contributions: from the bound (pn) intermediate state corresponding to a deuteron, where the separation energy is $E = E_D - E_{3\text{He}}$, with $E_{3\text{He}} \approx -7.72$ MeV the ${}^3\text{He}$ binding energy; and from the (pn) continuum scattering states. The neutron spectral function, on the other hand, has only the (pp) continuum contribution:

$$P^p(E, \mathbf{p}) = f^{p(d)}(\mathbf{p})\delta(E + E_{3\text{He}} - E_D) + f^{p(\text{cont})}(E, \mathbf{p}), \quad (7a)$$

$$P^n(E, \mathbf{p}) = f^{n(\text{cont})}(E, \mathbf{p}). \quad (7b)$$

A number of calculations of ${}^3\text{He}$ spectral function is available. In Ref.[21] this spectral function was obtained by solving the Faddeev equation with the Paris NN potential [22] for the ground state wave function, and constructing its projection onto the deuteron and two-body continuum states. In Ref.[23] the spectral function was obtained using a variational ${}^3\text{He}$ wave function calculated for a more recent AV14 NN potential. While in our numerical analysis we use the spectral functions from Ref.[21], we verified that both Ref.[21] and Ref.[23] lead to a consistent $\mathcal{R}({}^3\text{He}/{}^2\text{H})$ ratio.¹

For $A \geq 4$ nuclei we follow the model of Ref.[17], in which the full nuclear spectral function was calculated as a sum of the mean-field spectral function, describing a low-energy part of the separation energy spectrum, and the term generated by short-range NN correlations in the nuclear ground state responsible for a high separation energy and high-momentum component.

Nucleus	E_A/A	$\langle \varepsilon \rangle$	$\langle \mathbf{p}^2 \rangle / 2M$
${}^2\text{H}$	-1.11	-11.46	9.24
${}^3\text{He}$	-2.57	-17.95	12.87
${}^4\text{He}$	-7.07	-40.06	25.01
${}^9\text{Be}$	-6.46	-41.20	27.40
${}^{12}\text{C}$	-7.68	-45.35	28.83
${}^{14}\text{N}$	-7.48	-45.13	28.40

TABLE I. The nuclear binding energy per nucleon E_A/A , a bound nucleon energy ε and kinetic energy $\mathbf{p}^2/2M$ averaged with the nuclear spectral function normalized to one nucleon (all in MeV units).

In order to illustrate the evolution of the nuclear binding effect in light nuclei, in Table I we list the values of nuclear binding energy along with the average separation and kinetic energies of a bound nucleon for a few light nuclei. For the deuteron ${}^2\text{H}$ we use the Paris wave function, the parameters for ${}^3\text{He}$ were calculated using the spectral function of Ref.[21], whereas for $A \geq 4$ nuclei a model spectral function of Ref.[17] was used. Note a dramatic change in the energy parameters when going from ${}^3\text{He}$ to ${}^4\text{He}$, which is also the underlying reason of a difference in the magnitude of nuclear corrections to the structure functions, as will be discussed in Sec.III.

¹ In fact, the spectral functions of Ref.[21] and Ref.[23] result in an almost identical EMC ratio for $x < 0.85$. For $x > 0.85$ and Q^2 values of the E03-103 experiment, the calculation with the spectral function of Ref.[23] gives $\mathcal{R}({}^3\text{He}/{}^2\text{H})$ larger by some 1–2%. For the spectral function of Ref.[23] we used a more recent results with AV18 and Urbana IX potential (G. Salme, private communication).

B. Nucleon Structure Functions

In the DIS region, motivated by the twist expansion, the nucleon structure functions can be written as

$$F_2(x, Q^2) = F_2^{\text{TMC}}(x, Q^2) + H_2^{(4)}(x, Q^2)/Q^2 \quad (8)$$

where F_2^{TMC} is the leading-twist (LT) structure function corrected for the target mass effects and $H_2^{(4)}$ is the function describing the contribution of the twist-four terms. The LT structure functions are computed using the proton and neutron PDFs extracted from analysis of DIS and Drell-Yan data in a kinematical region of $Q^2 > 1 \text{ GeV}^2$ and invariant mass $W > 1.8 \text{ GeV}$ [24, 25] with the coefficient functions calculated to the NNLO approximation in the strong coupling constant in pQCD [26]. The target mass correction is computed following Ref.[27]. Although in general the twist expansion should include an infinite chain of the HT power terms, recent phenomenology suggests that Eq.(8) with only twist-four correction provides a good description of data down to $Q \sim 1 \text{ GeV}$ [15, 24, 25, 28]. It is also worth noting that this model is consistent with the duality principle and on average describes the resonance data with $W < 1.8 \text{ GeV}$ [15], which is relevant for the kinematical region of the JLab E03-103 experiment [12].

In calculating the nuclear structure functions one has to deal with the structure functions of the bound proton and neutron, which generally differ from those of the free proton and neutron. The effect of modification of bound nucleon SF is related to the dependence on the nucleon invariant mass p^2 in the off-shell region [see Eq.(2)]. One can separate the two sources of p^2 dependence: (i) The p^2 terms originating from the target mass effect in the off-shell region. The corresponding correction is of the order p^2/Q^2 . In Ref.[17] this effect is evaluated by the replacement $M^2 \rightarrow p^2$ in the expressions of Ref.[27]. (ii) The off-shell dependence of the the parton distributions (or LT structure functions); the latter effect is generally not suppressed by the inverse powers of Q^2 . In the description of this effect we treat the nucleon virtuality $v = (p^2 - M^2)/M^2$ as a small parameter, expand in series in v keeping the leading term:

$$F_2^{\text{LT}}(x, Q^2, p^2) = F_2^{\text{LT}}(x, Q^2) (1 + \delta f_2(x, Q^2) v), \quad (9)$$

$$\delta f_2 = \partial \ln F_2^{\text{LT}} / \partial \ln p^2, \quad (10)$$

where the first term on the right in Eq.(9) is the structure function of the on-mass-shell nucleon and the derivative is evaluated at $p^2 = M^2$.

Although the off-shell function (10) generally depends on the structure function type, it was suggested in Refs.[17, 18] that the relative off-shell effect (10) is common for all types of the nucleon PDFs. Thus, the function δf_2 measures a relative response of the nucleon parton distributions to the variation of the nucleon mass and, after the averaging with the nuclear spectral function, it describes the modification of the nucleon PDFs in the nuclear environment.

III. COMPARISON WITH DATA

We start this section by summarizing the results of our previous analysis [17] of data on the ratios of structure functions $\mathcal{R}(A/B) = F_2^A/F_2^B$ published before 1996. In Ref.[17] we performed a statistical analysis by calculating $\chi^2 = \sum (\mathcal{R}^{\text{exp}} - \mathcal{R}^{\text{th}})^2 / \sigma^2(\mathcal{R}^{\text{exp}})$, where \mathcal{R}^{exp}

Targets	χ^2/DOF						
	NMC	EMC	E139	E140	BCDMS	E665	HERMES
$^4\text{He}/^2\text{H}$	10.8/17		6.2/21				
$^7\text{Li}/^2\text{H}$	28.6/17						
$^9\text{Be}/^2\text{H}$			12.3/21				
$^{12}\text{C}/^2\text{H}$	14.6/17		13.0/17				
$^9\text{Be}/^{12}\text{C}$	5.3/15						
$^{12}\text{C}/^7\text{Li}$	41.0/24						
$^{14}\text{N}/^2\text{H}$							9.8/12
$^{27}\text{Al}/^2\text{H}$			14.8/21				
$^{27}\text{Al}/\text{C}$	5.7/15						
$^{40}\text{Ca}/^2\text{H}$	27.2/16		14.3/17				
$^{40}\text{Ca}/^7\text{Li}$	35.6/24						
$^{40}\text{Ca}/^{12}\text{C}$	31.8/24					1.0/5	
$^{56}\text{Fe}/^2\text{H}$			18.4/23	4.5/8	14.8/10		
$^{56}\text{Fe}/^{12}\text{C}$	10.3/15						
$^{63}\text{Cu}/^2\text{H}$		7.8/10					
$^{84}\text{Kr}/^2\text{H}$							4.9/12
$^{108}\text{Ag}/^2\text{H}$			14.9/17				
$^{119}\text{Sn}/^{12}\text{C}$	94.9/161						
$^{197}\text{Au}/^2\text{H}$			18.2/21	2.4/1			
$^{207}\text{Pb}/^2\text{H}$						5.0/5	
$^{207}\text{Pb}/^{12}\text{C}$	6.1/15					0.2/5	

TABLE II. Values of χ^2/DOF between different data sets with $Q^2 \geq 1 \text{ GeV}^2$ and the predictions of Ref.[17]. The normalization of each experiment is fixed. The sum over all data results in $\chi^2/\text{DOF} = 466.6/586$.

and \mathcal{R}^{th} are the data points and model predictions, respectively, and σ is the uncertainty of the experimental data points. The examined data come from different experiments for a variety of targets ranging from ^4He to ^{208}Pb with $Q^2 \geq 1 \text{ GeV}^2$ and in a wide region of Bjorken x (for a complete list of the analyzed data see Table 1 of Ref.[17]).

The ratio \mathcal{R}^{th} was calculated using approach outlined in Sec.II. We note that the calculations with Eq.(2) with the realistic nuclear spectral function, accounting for the Fermi motion and nuclear binding effect (FMB), and no off-shell correction explains a general trend of the EMC effect at large x values [29–31]. Nevertheless, the FMB effects alone fail to quantitatively describe data. In Ref.[17] a hypothesis was tested that the account of the off-shell effect in the bound nucleon SF would provide an accurate description of data. The function δf_2 was assumed to depend only on x which was then treated phenomenologically as a polynomial parametrization. Then the parameters, together with their uncertainties, were extracted from statistical analysis of data. This approach lead to an excellent agreement with all available data on $\mathcal{R}(A/B)$, reproducing the observed x , Q^2 , and A dependencies. In order to demonstrate the consistency between our model and the data, in Table II we list the values of χ^2/DOF obtained from data on different nuclei and from different experiments.

A. Data from nuclear targets with $A \geq 4$

More recent data on the nuclear EMC effect are available from HERMES experiment at HERA [8] and E03-103 experiment at JLab [12]. The HERMES experiment published the data for ${}^3\text{He}/{}^2\text{H}$, ${}^{14}\text{N}/{}^2\text{H}$ and ${}^{84}\text{Kr}/{}^2\text{H}$ ratios obtained with a 27.5 GeV positron beam for Bjorken x in the range $0.0125 < x < 0.35$ and an average Q^2 ranging from about 0.5 GeV^2 in a low x region to about 4 GeV^2 at large x . The E03-103 experiment published the measurements of ${}^3\text{He}/{}^2\text{H}$, ${}^4\text{He}/{}^2\text{H}$, ${}^9\text{Be}/{}^2\text{H}$, and ${}^{12}\text{C}/{}^2\text{H}$ ratios with a 5.77 GeV electron beam for x values ranging from 0.325 to 0.95 and an average Q^2 from about 3 GeV^2 at $x \sim 0.3$ to 6 GeV^2 at high x . In Fig.1 we summarize these data together with the former data by the NMC and SLAC E139 collaborations.

1. Consistency of different data sets

In this section we study the consistency of data from different experiments. From Fig.1 we can conclude that the slopes of the EMC ratio as a function of x from different experiments are in a good agreement. Note that the beam energy of these experiments differs significantly. As the beam energy determines the range of possible Q^2 values for each x -bin, the typical Q^2 values of the NMC experiment are significantly higher than those of the SLAC E139, HERMES, and JLab E03-103 experiments. Nevertheless, the data show no systematic Q^2 dependence of \mathcal{R} in the valence region $0.25 < x < 0.6$.

Contrary to the slope, the overall normalization factors of different experiments are not fully consistent. If we consider the ${}^{12}\text{C}$ and ${}^{14}\text{N}$ nuclei, which have a similar atomic number, we observe a good agreement in the normalizations of the NMC, SLAC E139, and HERMES experiments. However, the data points of the JLab E03-103 experiment are somewhat shifted above the data from other experiments. A similar trend is also present for the other nuclei, as can be seen from Fig.1. It is interesting to observe that for the double ratio $({}^9\text{Be}/{}^2\text{H})/({}^{12}\text{C}/{}^2\text{H})$ the normalization of the E03-103 data seems to agree with the SLAC E139 and NMC data. This fact points toward a common normalization offset for all ratios, possibly related to a common source of systematic uncertainty. It should be noted that the overall normalization uncertainty is not shown in Fig.1 but is summarized in Table III. The NMC experiment achieved the most precise absolute normalization within 0.4%, followed by the SLAC E139 experiment. For this reason we try to use NMC data as a reference and we evaluate the consistency of other experiments with NMC. From Fig.1 we can see that the statistical uncertainties of NMC data become large at $x > 0.3$ and therefore we can have an accurate comparison only in the region $0.1 < x < 0.3$. Following this observation, we proceed in two steps. First, we study the consistency of SLAC E139 and HERMES data with NMC in this overlap region. Then we compare the E03-103 data with SLAC E139 data since those two experiments have a broader overlap region for $x > 0.3$.

In order to evaluate the compatibility in the overall normalization factors of different experiments we follow a χ^2 approach. We consider the data shown in Fig.1 in the region $0.1 < x < 0.7$ and we rebin the measurements with a common bin size of 0.1/bin (six bins in total from 0.1 to 0.7). Within each larger bin, we calculate the weighted average of the data points from each experiments with weights given by $1/\sigma^2$. For each pair of experiments, we then calculate the corresponding χ^2 in the overlap region assuming a fixed normalization, as reported by the experiments. The results are summarized in Tables IV and V. From Table IV we can conclude that the three experiments NMC, SLAC E139 and HERMES

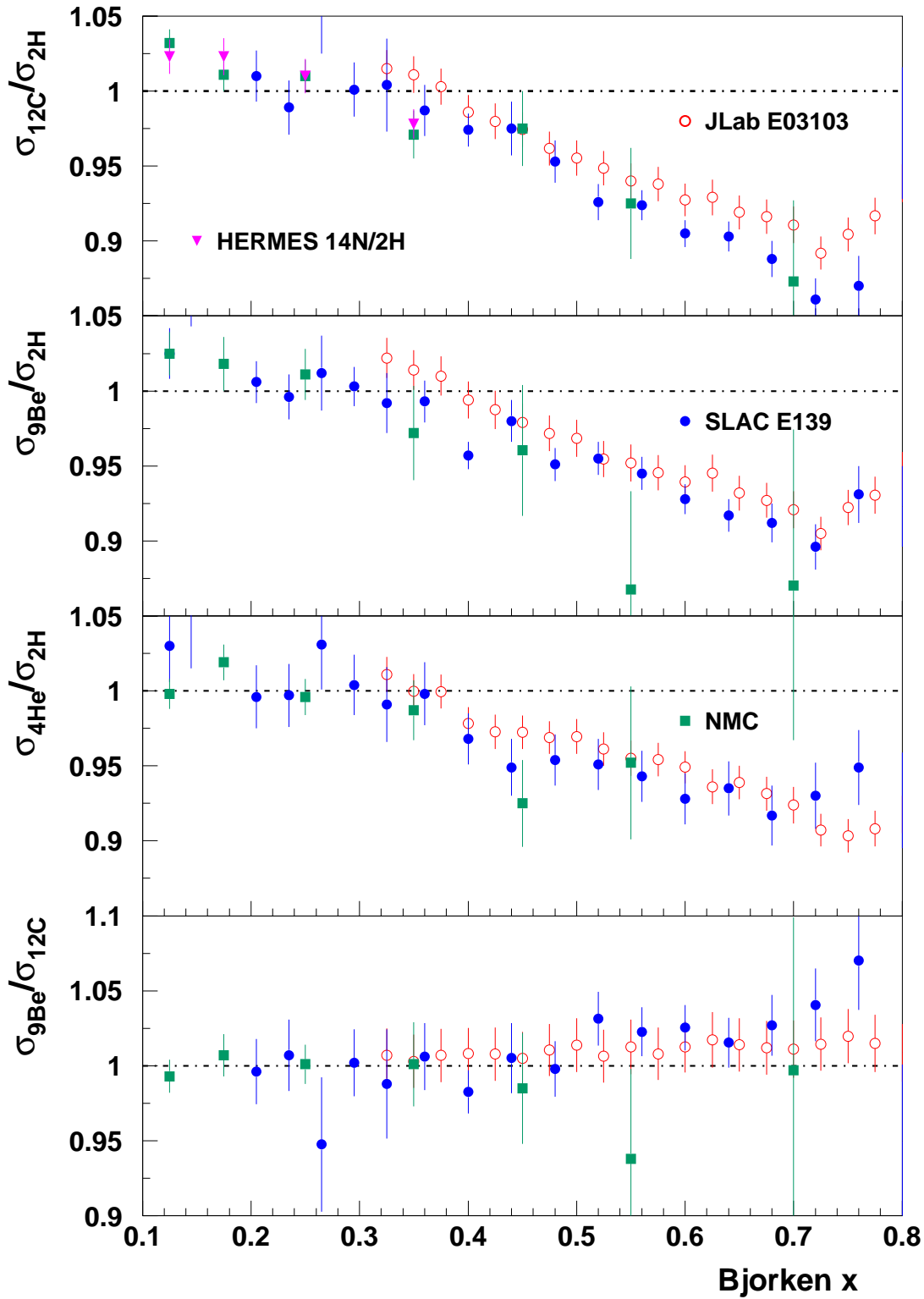


FIG. 1. (Color online) The \mathcal{R} -ratios of ^{14}N , ^{12}C , ^9Be , ^4He with respect to deuterium and the ratio $^9\text{Be}/^{12}\text{C}$ as measured by the NMC [4–6] (full squares), SLAC E139 [7] (full circles), JLab E03-103 [12] (open circles) and HERMES [8] (full triangles) experiments. Statistical and systematic uncertainties are added in quadrature, while the normalization uncertainty is not shown. For the E139 and E03-103 experiments the ratio $^9\text{Be}/^{12}\text{C}$ is calculated as a double ratio of data on $^9\text{Be}/^2\text{H}$ and $^{12}\text{C}/^2\text{H}$.

Targets	NMC	SLAC E139	HERMES	JLab E03-103
${}^3\text{He}/{}^2\text{H}$			1.4%	1.84%
${}^4\text{He}/{}^2\text{H}$	0.4%	2.4%		1.5%
${}^9\text{Be}/{}^2\text{H}$	0.4%	1.2%		1.7%
${}^{12}\text{C}/{}^2\text{H}$	0.4%	1.2%	1.4% (${}^{14}\text{N}/{}^2\text{H}$)	1.6%

TABLE III. Overall normalization uncertainties on the ratios \mathcal{R} from different experiments.

Experiment	SLAC E139	NMC	HERMES
	χ^2/DOF for ${}^{12}\text{C}/{}^2\text{H}$:		
SLAC E139		0.7/3	0.2/2
NMC			0.1/3
	χ^2/DOF for ${}^9\text{Be}/{}^2\text{H}$:		
SLAC E139		0.7/3	
	χ^2/DOF for ${}^4\text{He}/{}^2\text{H}$:		
SLAC E139		2.2/3	

TABLE IV. Compatibility between SLAC E139, NMC and HERMES data in the region $0.1 < x < 0.5$. The data shown in Fig.1 have been rebinned with a bin size of 0.1 for all experiments. The normalization of each experiment is fixed. The normalization uncertainties are not included in the evaluation of χ^2 .

χ^2/DOF between SLAC E139 and JLab E03-103				
	${}^4\text{He}/{}^2\text{H}$	${}^9\text{Be}/{}^2\text{H}$	${}^{12}\text{C}/{}^2\text{H}$	Total
Default normalization	4.6/4	21.7/4	16.4 /4	42.7/12
Normalization factor 0.98	1.1/4	6.4/4	1.3/4	8.8/12

TABLE V. Compatibility between SLAC E139 and JLab E03-103 data in the region $0.3 < x < 0.7$. The data shown in Figure 1 have been rebinned with a bin size of 0.1 for all experiments. In the second row all JLab data have been rescaled by an overall factor 0.98. The normalization uncertainties are not included in the evaluation of χ^2 .

Targets	χ^2/DOF	Normalization factor	Normalization uncertainty	χ^2/DOF w/o offset
${}^4\text{He}/{}^2\text{H}$	11.9/20	$1.9 \pm 0.3\%$	1.50%	23.6/21
${}^9\text{Be}/{}^2\text{H}$	9.2/20	$2.0_{-0.5}^{+0.1}\%$	1.70%	23.0/21
${}^{12}\text{C}/{}^2\text{H}$	5.2/20	$2.1_{-0.5}^{+0.2}\%$	1.60%	27.0/21
All data	26.3/60			73.6/63

TABLE VI. Values of χ^2/DOF between JLab E03-103 data [12] with $W^2 > 2 \text{ GeV}^2$ ($x < 0.85$) and our predictions [17]. The overall normalization of each data set has been kept floating while the corresponding normalization uncertainty is not included in the χ^2 . For comparison, the last column shows the χ^2/DOF obtained without any normalization offset but including the normalization uncertainty to the evaluation of χ^2 .

appear to be statistically compatible in the absolute normalization. However, the picture differs substantially for the E03-103 experiment. The JLab kinematics largely overlaps with the SLAC E139 experiment and for this reason we calculate the overall χ^2 between these two measurements. The results shown in Table V signal on inconsistency in the normalization of data from these experiments. We found that an overall normalization factor of $0.98_{-0.003}^{+0.005}$, applied to the ${}^4\text{He}/{}^2\text{H}$, ${}^9\text{Be}/{}^2\text{H}$, and ${}^{12}\text{C}/{}^2\text{H}$ data of the E03-103 experiment, makes them statistically compatible with the SLAC E139 data, lowering χ^2 by $\Delta\chi^2 = 33.9$. Therefore, in the following comparisons we will apply an overall normalization factor of 0.98 to the measurements ${}^4\text{He}/{}^2\text{H}$, ${}^9\text{Be}/{}^2\text{H}$ and ${}^{12}\text{C}/{}^2\text{H}$ from Ref. [12].

2. Comparison with model predictions

Figure 2 shows a comparison of our calculations with HERMES data [8] and also ${}^{12}\text{C}/{}^2\text{H}$ data from NMC experiment. These data emphasize the region of small x where the major nuclear correction is due to nuclear shadowing. We found a good agreement of model calculations with data over the whole kinematical region of x and Q^2 . We note that the shadowing effect arise in our model due to medium effects in the propagation of hadronic component of the virtual photon in nuclear environment. The magnitude of the shadowing effect is driven by the total cross section of scattering of hadronic component off a bound nucleon. This quantity strongly depends on Q^2 in the region of low Q^2 [17], which is the underlying reason for the difference in the shadowing correction for the NMC and HERMES data in Fig.2. We note that characteristic Q^2 are significantly smaller for the HERMES experiment. For example, in the x -bin 0.018 the average Q^2 is 2.9 GeV^2 for NMC and about 0.66 GeV^2 for HERMES. It should be also noted that pQCD and the twist expansion approach employed in Eq.(8) is out of the region of applicability for such low values of Q^2 . In order to evaluate the structure functions and their ratios at low Q^2 , we apply the spline extrapolation of Eq.(8) from the region $Q^2 \geq 1 \text{ GeV}^2$ to $Q^2 \rightarrow 0$ using the requirements from the conservation of the electromagnetic current [17]. We also note that a bump in the EMC ratio between $x = 0.1$ and 0.3 is due to an interplay between the nuclear shadowing and pion correction effects.

In Fig.3 we show a detailed comparison of our predictions with the E03-103 data for the ratios ${}^4\text{He}/{}^2\text{H}$, ${}^9\text{Be}/{}^2\text{H}$, and ${}^{12}\text{C}/{}^2\text{H}$. For each x bin, the ratios of nuclear cross sections were calculated at the average Q^2 value provided by the E03-103 experiment [12]. After applying the normalization factor of 0.98, required to match the NMC, E139 and HERMES data, we observe a very good agreement between our model and the E03-103 experiment for $x < 0.85$. Table VI lists the results of calculation of χ^2 between the model predictions and the data with and without renormalization. As a cross check, we also list the values of a normalization factor minimizing χ^2 if we leave the normalization floating for each of the three ratios ${}^4\text{He}/{}^2\text{H}$, ${}^9\text{Be}/{}^2\text{H}$, and ${}^{12}\text{C}/{}^2\text{H}$ from the E03-103 experiment. Note that the 2% offset appears statistically compatible with the overall normalization uncertainties quoted by the E03-103 experiment. Indeed, if we keep fixed the JLab normalization and we rather add the corresponding normalization uncertainties into the χ^2 calculation, we obtain a normalized χ^2 of 1.17. We also remark that allowing the normalizations to float reduces the χ^2/DOF to significantly less than unity that may signal an issue with the quoted uncertainties on the data.

In the region of $x > 0.85$ our calculations somewhat underpredict the E03-103 data. We note that in this region the data of Ref.[12] have $W^2 < 2 \text{ GeV}^2$ and therefore lie

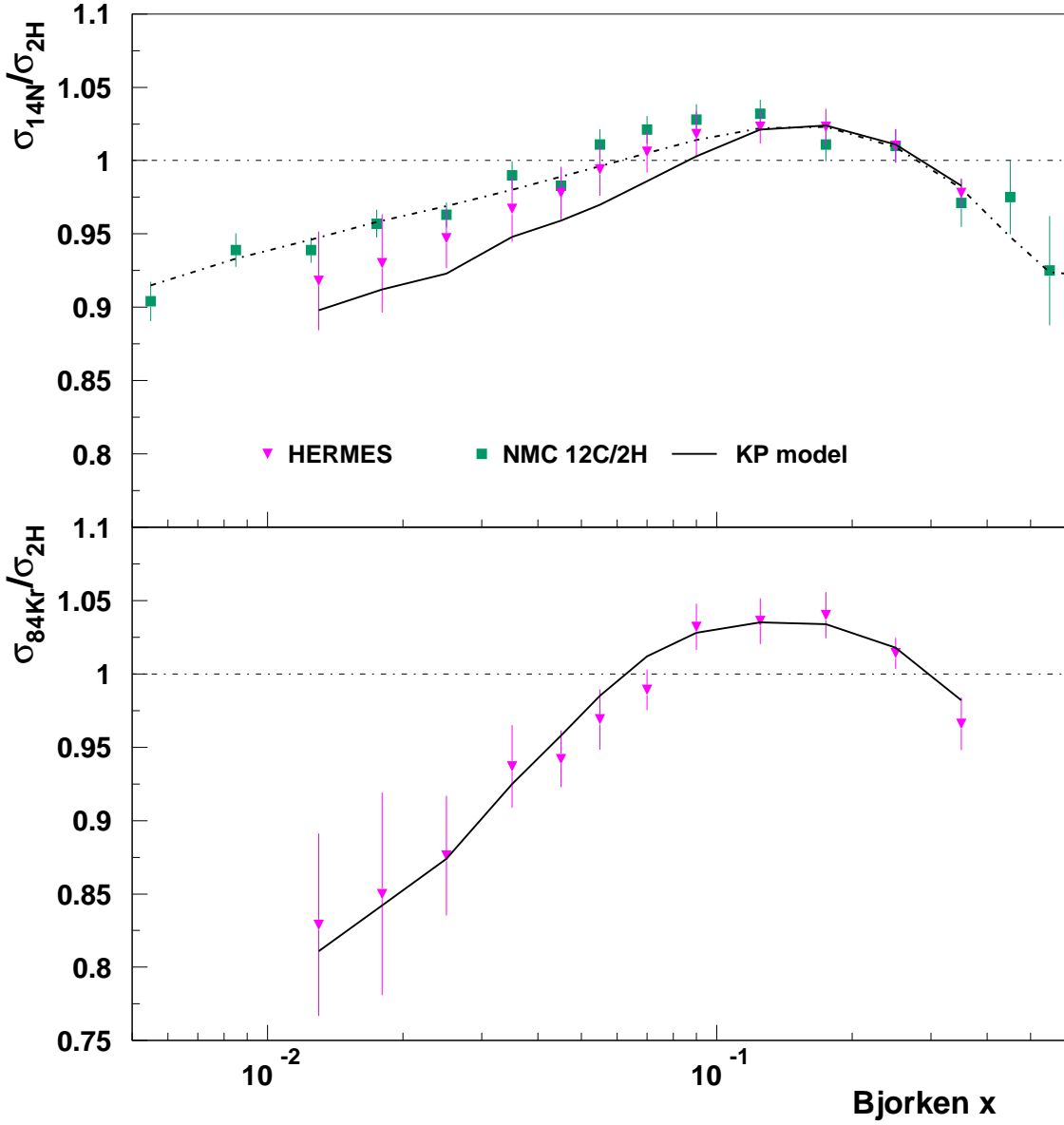


FIG. 2. (Color online) Ratios of cross sections for positron scattering off ^{14}N and ^{84}Kr nuclear targets with respect to a deuterium target. Data from the HERMES experiment [8] (full triangles) are compared with predictions of Ref.[17] calculated for the same kinematics (solid lines). Statistical and systematic uncertainties are added in quadrature, while the normalization uncertainty is not shown. The data from the NMC experiment for ^{12}C target and the results of Ref.[17] (dash-dotted line) are also shown in the top panel to illustrate the effect of the Q^2 dependence at low x values (see text).

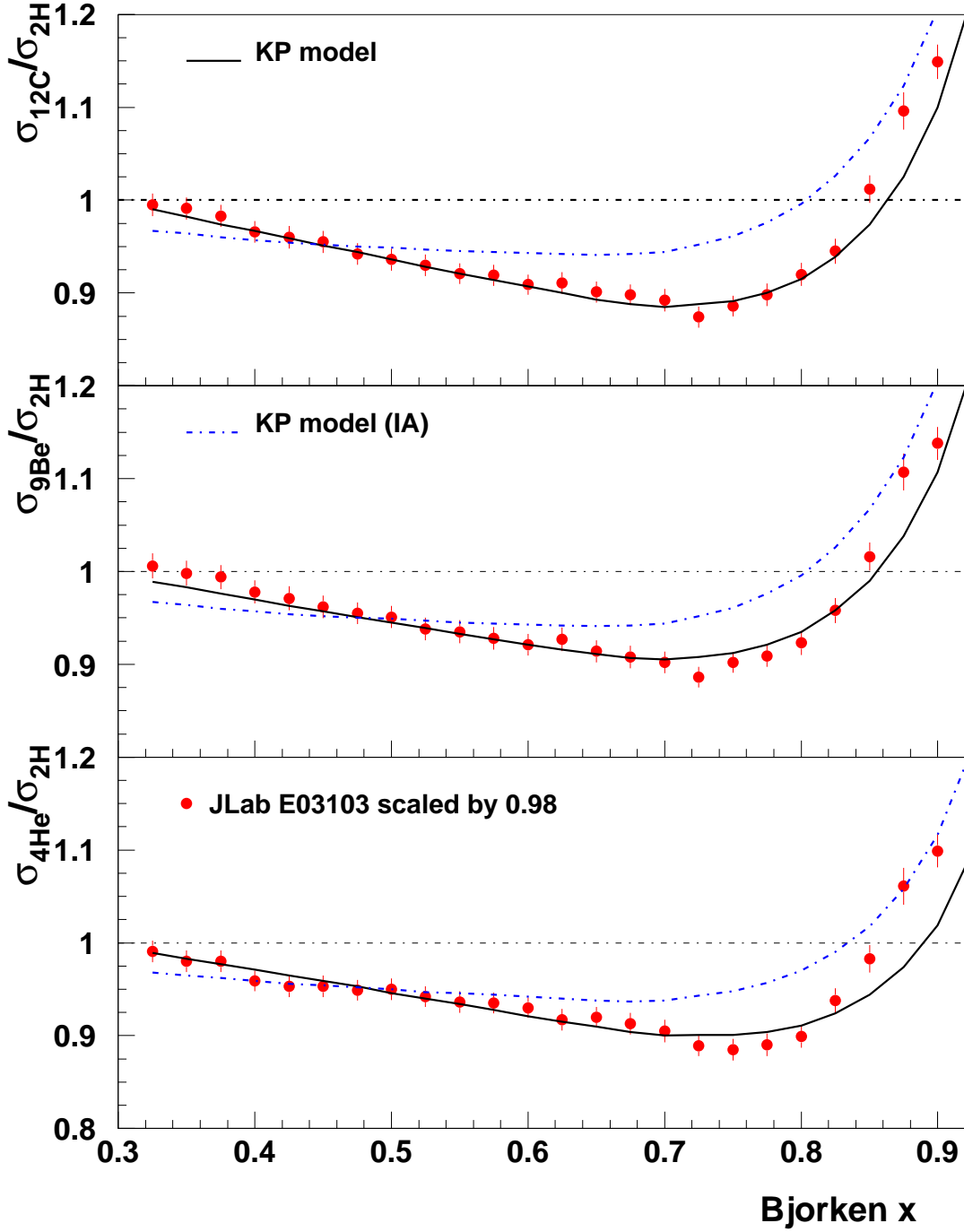


FIG. 3. (Color online) Data on the \mathcal{R} ratios of ^{12}C , ^9Be , and ^4He with respect to deuterium compared with predictions of the model of Ref.[17] for the same kinematics. A common normalization factor of 0.98 has been applied to all data points of Ref.[12], and statistical and systematic uncertainties are added in quadrature. The result of a calculation in impulse approximation with no off-shell correction is also shown as dashed-dotted line for comparison.

within the resonance region, while in our calculations we use a DIS model for the structure functions. Although we verified the consistency of low- Q DIS structure functions with the duality principle, a more detailed comparison would require explicit resonance model for the structure functions. Furthermore, the region of $x > 0.85$ is very sensitive to the treatment of both the bound nucleon momentum distribution and the target mass correction to the nucleon structure functions [17]. In our model, we apply the target mass correction following a commonly used method of Ref.[27]. However, it is known that the target mass correction of Ref.[27] leads to an incorrect behavior of SF in the limit of $x \rightarrow 1$ that has a significant impact on the calculation of nuclear ratio \mathcal{R} at very large x values. We also note that in the detailed comparison with the data the quasielastic contribution, which is not addressed in this article, may not be negligible in this region.

Finally, Fig.3 shows the results obtained with and without ($\delta f_2 = 0$) off-shell correction. We recall that the off-shell function δf_2 was determined in the former analysis of data [17]. We conclude that the off-shell correction plays a crucial role in understanding the data, implying the EMC effect is largely driven by the modification of properties of the bound nucleons inside the nuclei.

B. Data from ^3He target and the ratio F_2^n/F_2^p

Here we discuss nuclear effects in the ^3He target and further address the problem of consistency between data from different experiments. The EMC effect in the ^3He nucleus was measured by HERMES [8] and recently at JLab [12]. We recall that the data are presented in a form corrected for the proton–neutron difference in a nucleus, as discussed in Sec.II. The isoscalar correction depends on the ratio F_2^n/F_2^p and for this reason a direct comparison of corrected data is biased by the models used in different experiments. The uncorrected data on the EMC ratios are available from Ref.[12] and comparison with those data allows us to reduce a bias associated with the isoscalar correction.

In the former discussion we addressed possible inconsistency in the normalization of the EMC ratios from different experiments. Below we discuss the relation between the ratios $\mathcal{R}(^3\text{He}/^2\text{H}) = \frac{1}{3}F_2^{3\text{He}}/\frac{1}{2}F_2^D$ and $\mathcal{R}(^2\text{H}/^1\text{H}) = \frac{1}{2}F_2^D/F_2^p$ and F_2^n/F_2^p , and will argue that the comparison of the F_2^n/F_2^p ratio extracted from $^3\text{He}/^2\text{H}$ data of the E03-103 experiment [12] and the $^2\text{H}/^1\text{H}$ data by NMC [32] provides a sensitive test of the normalization of the $^3\text{He}/^2\text{H}$ data.

In the absence of nuclear effects, the ratio F_2^n/F_2^p can directly be calculated from either the $^2\text{H}/^1\text{H}$ or $^3\text{He}/^2\text{H}$ ratio. A realistic analysis should include the treatment of nuclear effects. Let us first consider the ratio $^2\text{H}/^1\text{H}$. In order to address the nuclear corrections in this problem, it is convenient to consider the ratio $R_2 = F_2^D/(F_2^p + F_2^n)$ and recast F_2^D in terms of R_2 . We have for F_2^n/F_2^p :

$$F_2^n/F_2^p = 2\mathcal{R}(^2\text{H}/^1\text{H})/R_2 - 1. \quad (11)$$

Addressing the ratio $^3\text{He}/^2\text{H}$, we need to consider $R_3 = F_2^{3\text{He}}/(2F_2^p + F_2^n)$ along with R_2 . We recast $F_2^{3\text{He}}$ in terms of R_3 and after a simple algebra we have:

$$F_2^n/F_2^p = (2 - z)/(z - 1), \quad (12)$$

where $z = \frac{3}{2}\mathcal{R}(^3\text{He}/^2\text{H})R_2/R_3$.

In Fig. 4 we show the results of extraction of F_2^n/F_2^p from the NMC and the E03-103 data using Eqs. (11) and (12). It should be remarked that a typical region of Q^2 is significantly higher in the NMC experiment than that of the E03-103 experiment at JLab. Nevertheless, Ref. [32] presents the results for the Q^2 dependence of the $^2\text{H}/^1\text{H}$ ratio. In order to reduce a bias due to Q^2 dependence, in our analysis we use the NMC parametrization of Q^2 dependence of their data and select the values of Q^2 close to those of Ref.[12].

In order to test the impact of nuclear effects on the extraction of F_2^n/F_2^p , we performed the analysis with the full treatment of nuclear effects and also with no nuclear effects included, i.e., assuming $R_2 = R_3 = 1$. Both results are shown in Fig.4. The ratios R_2 and R_3 , used in the full analysis, are shown in Fig.5. The ratio R_2 was calculated as described in Ref.[17] using the proton and neutron structure functions of Refs.[15, 33] and the Paris deuteron wave function [22], while the ^3He structure function and the ratio R_3 was calculated by Eq.(2) using the spectral function of Ref.[21] (see Sec.IIA). We observe from Fig. 5 that the EMC effect in R_3 is similar to that in R_2 with the minimum at $x \sim 0.7$ being somewhat deeper for R_3 . Note that the nuclear effects cancel in the region $x \sim 0.35$, which is consistent with the measurements of the EMC effect on other nuclei.

A significant mismatch in the values of F_2^n/F_2^p extracted from different experiments is indicated in Fig. 4. In particular, at $x = 0.35$ the central point of the F_2^n/F_2^p ratio from $^3\text{He}/^2\text{H}$ data needs to be rescaled by a factor $0.85_{-0.03}^{+0.04}$ with respect to the corresponding value from the $^2\text{H}/^1\text{H}$ data. In this region the extraction of F_2^n/F_2^p from nuclear data is practically unaffected by nuclear effects, as illustrated in Fig. 4. Note, however, that for larger x the nuclear corrections are significant. Curiously enough, the sign of nuclear effect on the ratio F_2^n/F_2^p extracted from $^3\text{He}/^2\text{H}$ differs from that extracted from the $^2\text{H}/^1\text{H}$ ratio. This is because the dependence on R_2 in Eq.(11) and the dependence on R_2/R_3 in Eq.(12) essentially differ. Note also that in the case of $^3\text{He}/^2\text{H}$ the nuclear effects come through the ratio R_2/R_3 thus reducing the impact of the Fermi motion at large x .

The normalization of F_2^n/F_2^p is directly related to the normalization of the $^3\text{He}/^2\text{H}$ data and the observed mismatch may signal an inconsistency in the normalization of nuclear data. We apply Eq.(12) to evaluate necessary renormalization of $\mathcal{R}(^3\text{He}/^2\text{H})$ in order to match the F_2^n/F_2^p ratio from $^2\text{H}/^1\text{H}$ data and find that the $^3\text{He}/^2\text{H}$ ratio should be increased by a factor $1.03_{-0.008}^{+0.006}$.

In order to further study the nuclear data normalization issue, in Fig. 6 we compare the $^3\text{He}/^2\text{H}$ data from the HERMES [8] and JLab E03-103 [12] experiments. The HERMES data have been corrected for the proton excess using a correction factor in Eq.(5) with $F_2^{p,n}$ from the NMC measurements. The open circles correspond to the ‘‘isoscalar’’ data as provided in Ref. [12]. The filled circles stand for the E03-103 data corrected for nonisoscality in a different way: We first obtain a raw data by removing the isoscalarity correction of Ref. [12] and then apply the factor C_{is} by Eq.(5) with F_2^p and F_2^n of Ref. [15, 33] calculated for each x bin. In addition we also apply a renormalization factor of 1.03 to each data point. Also shown are the results of our calculations of $C_{is}\mathcal{R}(^3\text{He}/^2\text{H})$. It is worth noting that the isoscalarity correction factor C_{is} differs significantly from the corresponding correction in Ref.[12] and we illustrate its model dependence in Fig.7. In order to avoid confusion caused by different correction factors, in Fig. 6 we compare the calculations with the data corrected in a similar way. We find from Fig.6 that at the overlap region at $x = 0.35$, such renormalized E03-103 data are in a good agreement with HERMES data.

Finally, we note that the nuclear effects in ^3He are significantly smaller than in ^4He (cf. Fig.3 and Fig.6). Such a difference is naturally explained in our approach by a dramatic

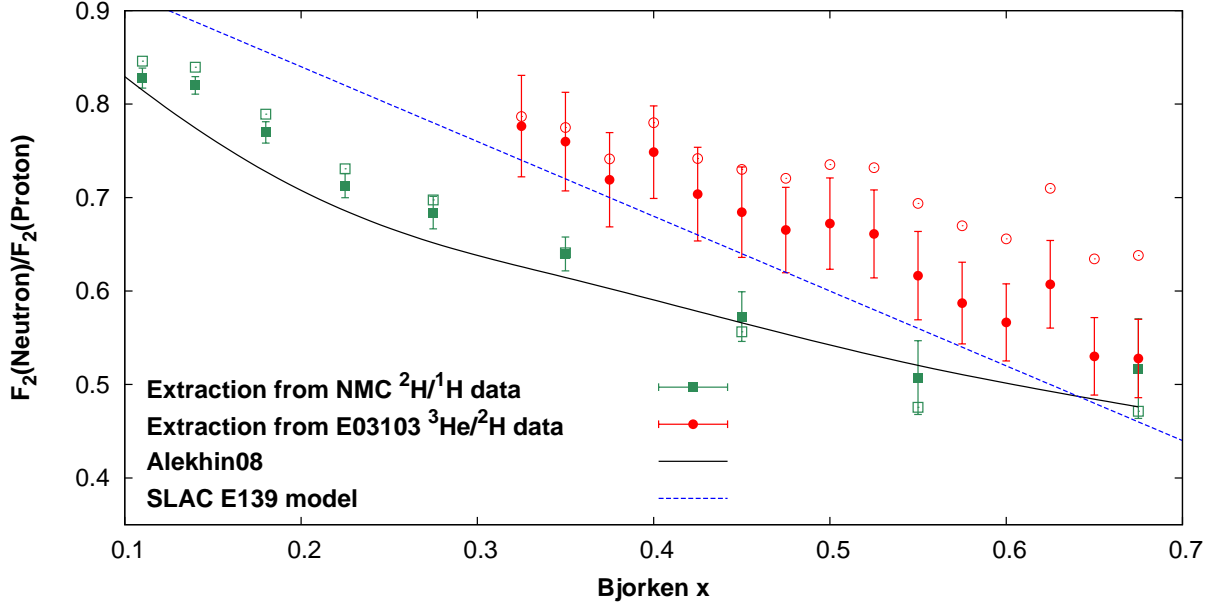


FIG. 4. (Color online) The results of the extraction of the ratio F_2^n/F_2^p from data on the $^2\text{H}/^1\text{H}$ cross-section ratio by the NMC experiment [32] (green squares) and the data on the $^3\text{He}/^2\text{H}$ cross-section ratio by JLab E03-103 experiment [12] (red circles). The full symbols are obtained with the model of nuclear effects of Ref.[17], while the open symbols show the points obtained with no nuclear corrections. The solid curve is the result of a calculation according to Eq.(8) with the NNLO PDFs and the HT corrections of Refs. [15, 25, 33], for the Q^2 corresponding to the NMC kinematics. The dashed line is a Q^2 independent model used in Ref.[7].

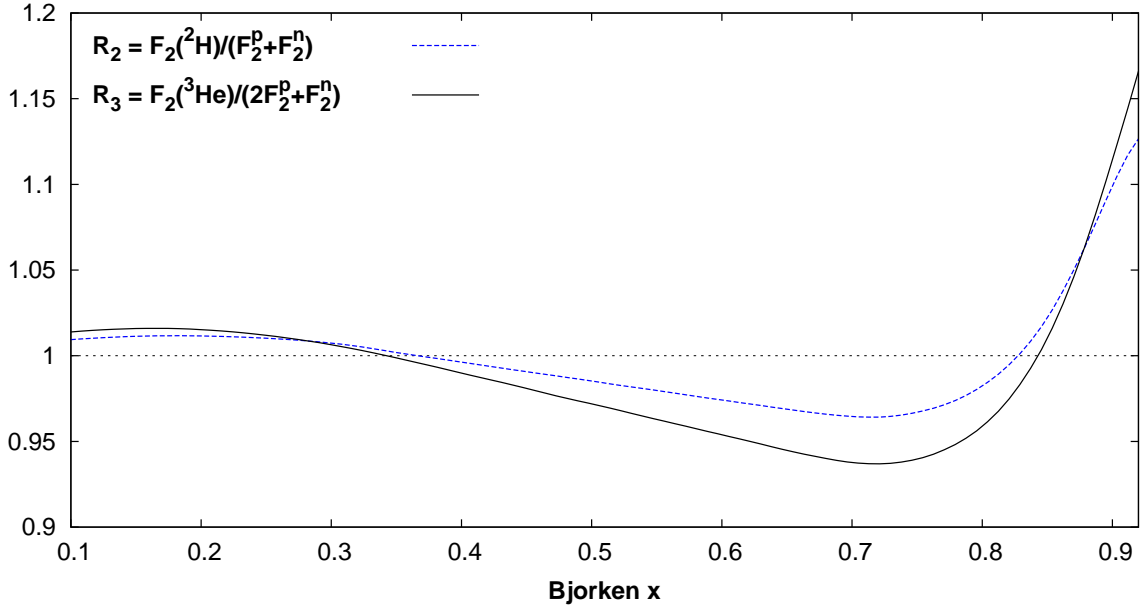


FIG. 5. (Color online) The ratios R_2 and R_3 calculated at the values of x and Q^2 of Ref.[12] for $x > 0.3$ and at fixed $Q^2 = 3 \text{ GeV}^2$ for $x < 0.3$.

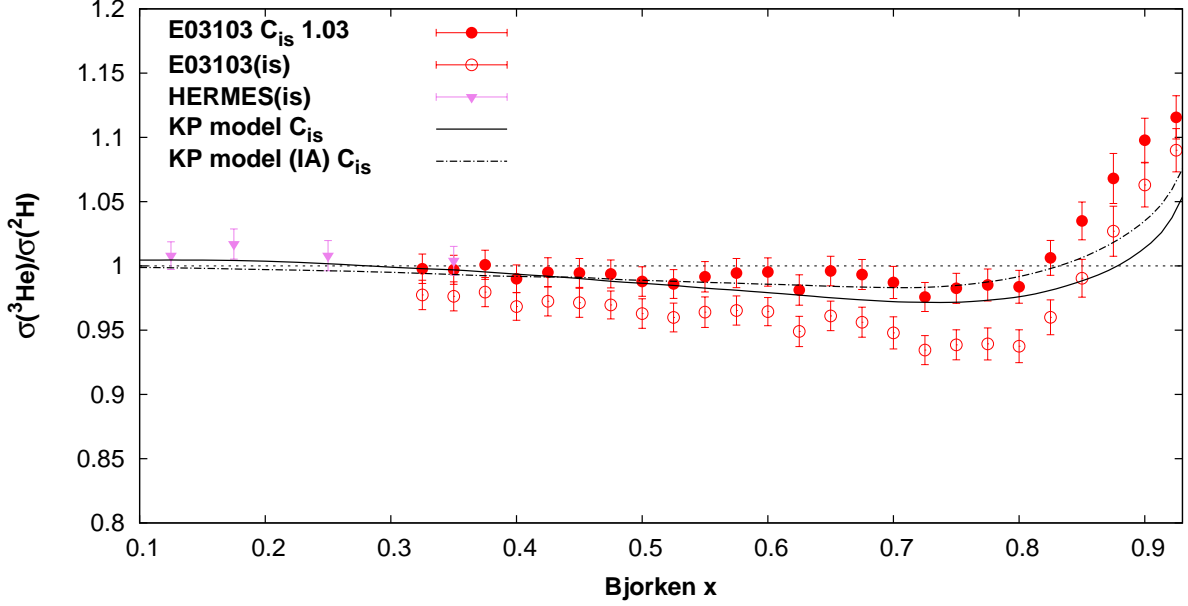


FIG. 6. (Color online) Ratio of cross sections for electron scattering off ${}^3\text{He}$ with respect to a deuterium target, corrected for the proton excess. Data from the HERMES experiment [8] (triangles) and the JLab E03-103 experiment [12] (open circles) are compared with the E03-103 raw data renormalized by a factor 1.03 and corrected for the proton excess according to Eq.(5) and using the proton and neutron structure functions of Refs. [15, 33] (full circles). Our predictions calculated for the same kinematics with the complete model described in this article (solid line) and in the impulse approximation (dashed line) are also shown for comparison. See text for details.

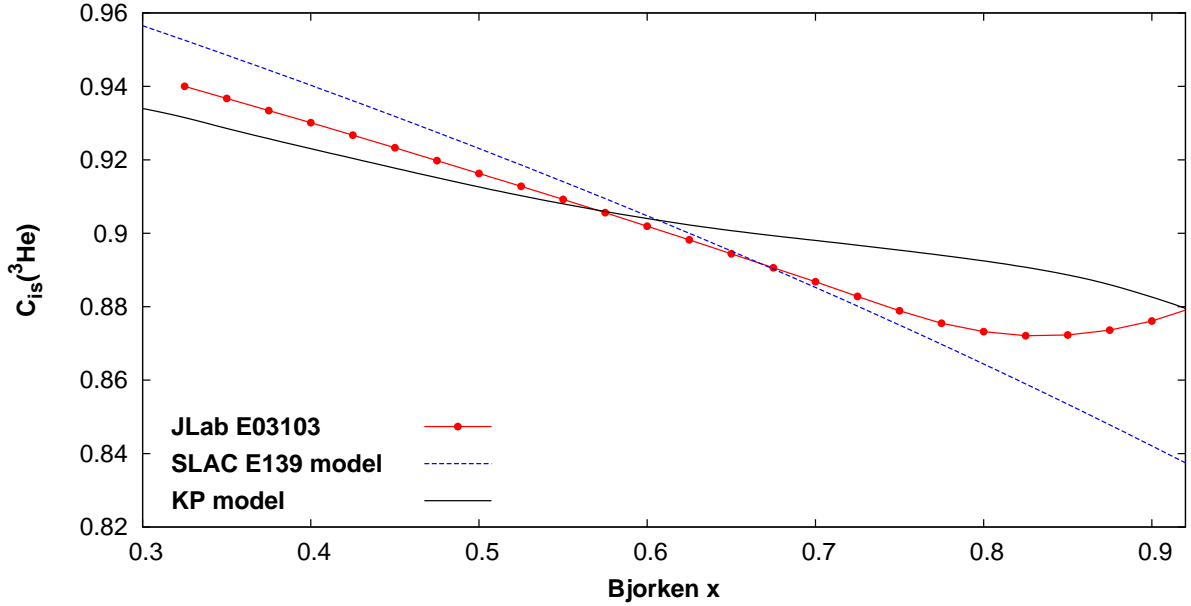


FIG. 7. (Color online) The isoscalar correction for ${}^3\text{He}$ calculated by Eq.(5) using different models of F_2^n/F_2^p .

difference in nuclear binding for these two nuclei, as illustrated in Table I. The off-shell effect is also smaller in ${}^3\text{He}$ because its rate is controlled by the nucleon virtuality v [see Eq.(9)], whose value is driven by nuclear binding. Using Table I we obtain for average virtuality $v = -0.065$ (${}^3\text{He}$) and -0.14 (${}^4\text{He}$). Thus, a significantly larger value of $|v|$ for ${}^4\text{He}$ explains more pronounced off-shell effect in this nucleus.

IV. SUMMARY

We presented a detailed analysis of nuclear EMC effect for light nuclei. Focusing on the overlap region $0.1 < x < 0.7$, we perform a statistical χ^2 analysis of the consistency between the data sets from different experiments. We found a good agreement between the normalizations of the NMC, SLAC E139 and HERMES experiments for nuclei with $A \geq 4$. However, the points from the JLab E013-103 experiment appear systematically shifted above the SLAC E139 data by an overall normalization factor of $0.98_{-0.003}^{+0.005}$, common to all discussed nuclei with $A \geq 4$. This renormalization factor is statistically consistent with the normalization uncertainty quoted in Ref.[12]. After applying the normalization offset the JLab E013-103 data are in good agreement with both SLAC E139 and NMC data.

The predictions of Ref.[17] are in a good agreement with renormalized E013-103 data for all studied nuclei, as discussed in Sec.III A 2. We would like to emphasize an important role of off-shell correction, which is crucial in the description of both the slope of $\mathcal{R}(x)$ for $0.3 < x < 0.7$ and position of its minimum at $x \sim 0.75$. This correction is controlled by a product $\delta f_2(x)v$ averaged with the nuclear spectral function. The function $\delta f_2(x)$ measures a relative change in the nucleon structure function due to variation of its invariant mass. In Ref.[17] this function was phenomenologically derived from a data analysis on nuclear ratios \mathcal{R} . Further interpretation of observed behavior of $\delta f_2(x)$ in terms of detailed models would help to better understand mechanisms of modification of the partonic structure of the nucleon in nuclear environment.

The HERMES data on ${}^{14}\text{N}$ are consistent with the NMC data on ${}^{12}\text{C}$ at $x > 0.1$. The predictions by Ref.[17] agree with both experiments. We observe that at small x the shadowing effect is more pronounced in the HERMES data than in the NMC data. This difference can be attributed to the Q^2 dependence, since the average Q^2 of the HERMES experiment is significantly lower than the corresponding one of the NMC experiment. This effect is also confirmed by calculations in a model of Ref.[17].

A significant part of the present analysis is devoted to the study of the EMC effect in ${}^3\text{He}$, for which the data from both HERMES and JLab E03-103 experiments are available. In the overlap region at $x \sim 0.35$ the normalizations of the two experiments somewhat disagree. It is important to note that the data on nuclear ratios are usually corrected for the proton excess, which depends on the ratio F_2^n/F_2^p . For this reason, the data appear to be biased by different models of the isoscalarity correction. In order to verify the consistency of data, we study the relation between the ratios of nuclear structure functions and F_2^n/F_2^p . We extract F_2^n/F_2^p from both the E03-103 data on the ${}^3\text{He}/{}^2\text{H}$ ratio and the NMC data on the ${}^2\text{H}/{}^1\text{H}$ ratio. A significant difference between the results of these two extractions is observed. In particular, we find that at $x = 0.35$ and $Q^2 \approx 3 \text{ GeV}^2$ the ratio F_2^n/F_2^p obtained from the JLab E03-103 data is about 15% larger than that extracted from the NMC data. Both extractions of F_2^n/F_2^p become consistent once a normalization factor of $1.03_{-0.008}^{+0.006}$ is applied to the ${}^3\text{He}/{}^2\text{H}$ ratio of the E03-103 experiment. After such renormalization the E03-103 and HERMES data on the ${}^3\text{He}/{}^2\text{H}$ ratio also become consistent, and our predictions are in good

agreement with both data sets in the region $x < 0.85$.

V. ACKNOWLEDGEMENTS

We thank J. Arrington, A. Daniel and D. Gaskell for useful communications and information on the E03-103 experiment and C. Riedl for useful information on the HERMES data. We are also grateful to S. Alekhin, W. Melnitchouk and S. Scopetta for fruitful discussions and communications. R.P. thanks USC for supporting this research.

-
- [1] EMC, J. J. Aubert *et al.*, Phys. Lett. **B123**, 275 (1983).
 - [2] BCDMS, G. Bari *et al.*, Phys. Lett. **B163**, 282 (1985).
 - [3] EMC, J. Ashman *et al.*, Z. Phys. **C57**, 211 (1993).
 - [4] NMC, M. Arneodo *et al.*, Nucl. Phys. **B441**, 12 (1995).
 - [5] NMC, P. Amaudruz *et al.*, Nucl. Phys. **B441**, 3 (1995).
 - [6] NMC, M. Arneodo *et al.*, Nucl. Phys. **B481**, 3 (1996).
 - [7] E139, J. Gomez *et al.*, Phys. Rev. **D49**, 4348 (1994).
 - [8] HERMES, K. Ackerstaff *et al.*, Phys. Lett. **B475**, 386 (2000); Erratum-ibid. **B567**, 339 (2003).
 - [9] E665, M. R. Adams *et al.*, Z. Phys. **C67**, 403 (1995).
 - [10] M. Arneodo, Phys. Rept. **240**, 301 (1994).
 - [11] D. F. Geesaman, K. Saito, and A. W. Thomas, Ann. Rev. Nucl. Part. Sci. **45**, 337 (1995).
 - [12] E03-103, J. Seely *et al.*, Phys. Rev. Lett. **103**, 202301 (2009); see also the E03-103 experiment web resource <https://hallcweb.jlab.org/experiments/E03103/>.
 - [13] Y. Kahn, W. Melnitchouk, and S. A. Kulagin, Phys. Rev. **C79**, 035205 (2009).
 - [14] S. Alekhin, S. Kulagin, and R. Petti, (2009), arXiv:0910.3762.
 - [15] S. Alekhin, S. A. Kulagin, and R. Petti, AIP Conf. Proc. **967**, 215 (2007).
 - [16] S. Alekhin, S. Kulagin and R. Petti, Phys. Lett. B **675**, 433 (2009).
 - [17] S. A. Kulagin and R. Petti, Nucl. Phys. **A765**, 126 (2006).
 - [18] S. A. Kulagin and R. Petti, Phys. Rev. **D76**, 094023 (2007).
 - [19] B. L. Ioffe, V. A. Khoze, and L. N. Lipatov, *Hard Processes. Vol. 1: Phenomenology, Quark-Parton Model* (Elsevier, Amsterdam, 1984).
 - [20] S. A. Kulagin and W. Melnitchouk, Phys. Rev. **C78**, 065203 (2008).
 - [21] R. W. Schulze and P. U. Sauer, Phys. Rev. **C48**, 38 (1993).
 - [22] M. Lacombe *et al.*, Phys. Rev. **C21**, 861 (1980).
 - [23] A. Kievsky, E. Pace, G. Salme, and M. Viviani, Phys. Rev. **C56**, 64 (1997).
 - [24] S. Alekhin, Phys. Rev. **D68**, 014002 (2003).
 - [25] S. Alekhin, K. Melnikov, and F. Petriello, Phys. Rev. **D74**, 054033 (2006).
 - [26] E. B. Zijlstra and W. L. van Neerven, Nucl. Phys. **B383**, 525 (1992).
 - [27] H. Georgi and H. D. Politzer, Phys. Rev. **D14**, 1829 (1976).
 - [28] S. I. Alekhin, S. A. Kulagin, and S. Liuti, Phys. Rev. **D69**, 114009 (2004).
 - [29] S. V. Akulinichev, S. A. Kulagin, and G. M. Vagradov, Phys. Lett. **B158**, 485 (1985).
 - [30] S. V. Akulinichev, S. Shlomo, S. A. Kulagin, and G. M. Vagradov, Phys. Rev. Lett. **55**, 2239 (1985).

- [31] S. A. Kulagin, Nucl. Phys. **A500**, 653 (1989).
- [32] NMC, M. Arneodo *et al.*, Nucl. Phys. **B487**, 3 (1997).
- [33] S. Alekhin, S. Kulagin, and R. Petti, (2008), arXiv:0810.4893 [hep-ph].

